Title

Improving Efficiency, Stability, and Accuracy of Finite Element Solutions for Solving Dynamic Contact Problems Involving Unsaturated Soils

Permalink

ISBN

Authors

Ghorbani, Javad
Chen, Liuxin
Kodikara, Jayantha
et al.

Publication Date

2023

DOI

Peer reviewed

Improving efficiency, stability, and accuracy of finite element solutions for solving dynamic contact problems involving unsaturated soils

Javad Ghorbani[1*], Liuxin Chen[2], Jayantha Kodikara[2], John P. Carter[3] and John S. McCartney[4]

[1] ARC Smart Pavements Hub, Department of Civil Engineering, Monash University, VIC 3800.
Javad.ghorbani@monash.edu

[2] ARC Smart Pavements Hub, Department of Civil Engineering, Monash University, VIC 3800.

[3] School of Engineering, The University of Newcastle, NSW 2308, Australia.

[4] University of California, San Diego, La Jolla, CA 92093-0085, USA.

Abstract The paper investigates the efficiency, stability, and accuracy of finite element solutions based on the mortar approach in solving dynamic contact problems that involve unsaturated soils. We employ a fully coupled finite element solution and a recently developed bounding surface model for describing the hydro-mechanical hysteresis of unsaturated soils. The paper discusses a key source of instability in numerical simulations of this class of problems which is stress overshooting. We evaluate the efficiency of a solution for this problem and discuss the impact of this solution on improving the accuracy and stability of numerical simulations. Numerical simulations are presented for verification and analysis of efficiency, stability, and accuracy.

Keywords: Stress overshooting, unsaturated soils, dynamics, plasticity, finite element analysis, Contact mechanics

1 Introduction

Contact problems are highly non-linear and one of the most challenging problems in computational mechanics (Wriggers and Laursen, 2006). Compared to materials such as steel, soils often exhibit a very limited elasticity range and their behavior depends on factors such as the presence of water inside their pores, hydraulic hysteresis, shear strain amplitude, and drainage conditions (Khosravi and McCartney, 2012, Kodikara et al., 2018, Airey and Ghorbani, 2021, Dong et al., 2018, Rong and McCartney, 2021, Rong and McCartney, 2020). Including these aspects in geotechnical analyses increases the degree of nonlinearity. Therefore, the robustness and unconditional

stability of numerical solutions cannot be guaranteed (De Borst et al., 2012). In this regard, improving the stability of numerical solutions is important as geotechnical applications of contact mechanics become more complex.

In recent years, there is a growing interest in assessing the serviceability of critical infrastructure resting on unsaturated soils, such as road networks and onshore wind turbines. In this class of problems, the quality of design can be improved by developing novel numerical solutions based on contact mechanics where the interaction between structural elements such as wheel and foundations and unsaturated soils can be accurately represented. Such solutions will improve the accuracy of predictions of the loads that are transferred between structural elements and unsaturated soils. Furthermore, if coupled with appropriate constitutive models, these numerical solutions can facilitate accurate assessments of ratcheting of unsaturated soils under cyclic interactions as well as the ability (or inability) of these soils to reach the shakedown state (Rong and McCartney, 2019). Also, such solutions can assist in improving ground compaction practices to ensure serviceability and reasonable performance during cyclic loading.

This paper explores the efficiency of a method to improve the stability of numerical solutions to dynamic interactions with unsaturated soils. Since the 1990s, there has been a quest for efficient constitutive models that can present a unified description of the response of unsaturated soils under monotonic and cyclic loads. One of the major numerical problems associated with these models is the issue of stress overshooting which can arise when numerical oscillations are wrongly interpreted as true cyclic loads by the model. In this condition, the plastic modulus experiences a drastic change in response to oscillations, leading to premature termination of the analysis. Oscillations are very common in dynamic contact problems, therefore, finding efficient remedies to the overshooting effect can significantly improve the stability of numerical solutions to this class of contact problems. We will begin by introducing the constitutive model and the issue of overshooting and giving numerical examples of the issue. An approach to mitigate this issue together with its performance in numerical simulations of contact problems will be discussed later.

2 Constitutive model

In this paper, a recently developed soil model for unsaturated soils termed MUD (Model for Unsaturated soil Dynamics) (Ghorbani et al., 2021a) will be used. MUD eliminates the need to enforce the consistency conditions at the end of the integration process; a feature that simplifies the stress integration algorithm (Ghorbani et al., 2021a). This is obtained by eliminating the purely elastic region and defining a loading surface on which the stress state is always located. The model can simulate soil behaviour under a wide range of hydro-mechanical loads by considering the impact of stress-induced anisotropy on volumetric and deviatoric hardening laws. In addition, a

combination of Bishop's effective stress (by taking the Bishop's parameter as the degree of saturation (Schrefler, 1984)) and the "bonding variable", ξ (Gallipoli et al., 2003) is used to model hardening/softening induced by the changes in the degree of saturation (or suction). ξ is a scalar quantity and denotes the average intergranular force generated by the presence of water menisci in the soil skeleton and is defined as

$$\xi = \left(1 - S_w\right) g\left(\widetilde{p}_c\right) \tag{1}$$

where $\widetilde{p}_c$ is the suction, p_c, normalised with respect to the atmospheric pressure. $g\left(\widetilde{p}_c\right)$ describes the intergranular force exerted by the water meniscus. This can be approximated as the force acting between two identical spheres, for which the hyperbolic formula given in (Borja, 2004) is used, i.e., $g\left(\widetilde{p}_c\right) = 1 + \dfrac{\widetilde{p}_c}{10.7 + 2.4\,\widetilde{p}_c}$.

The model uses the concept of the "state parameter" (Been and Jefferies, 1985) that enables a unified description of the response of granular soils at different initial void ratios.

With reference to elastic response, the equation of the bulk modulus, K and shear modulus, G (based on the suggestions of (Taiebat and Dafalias, 2008) for fully saturated soils) are generalised to unsaturated states by using Bishop's effective stress (Chen et al., 2021, Ghorbani and Airey, 2021) as follows

$$K = K_0\, p_{atm} \frac{1+e}{e} \left(\frac{p^{'}}{p_{atm}}\right)^{\frac{2}{3}} \tag{2}$$

where $p^{'}$ is the mean effective stress, e is the void ratio, p_{atm} is the atmospheric pressure, and K_0 is a material parameter. The shear modulus, G, is defined by Richart et al., (1970)

$$G = G_0\, p_{atm} \frac{\left(2.97 - e\right)^2}{1+e} \left(\frac{p^{'}}{p_{atm}}\right)^{\frac{1}{2}} \tag{3}$$

where G_0 is a model parameter. It may be notd that the coeeficient of (1/2) can be taken as a material parameter as suggested by Khosravi and McCartney (2009). Nonetheless, to reduce the number of parameters, in this study, we take it as a contant following (Taiebat and Dafalias, 2008). Isotropic hardening parameter, α_{iso}^{l} can evolve in response to the changes in the plastic volumetric strain, ε_{v}^{p} according to

$$d\,\alpha_{iso}^{l} = \frac{\left(1+e\right)}{e} \frac{\alpha_{iso}^{l}\left(1+C\right)}{\left(\left(\lambda - \kappa\right) F\left(\delta_p\right) - \kappa C\right)} d\,\varepsilon_{v}^{p} + \frac{\alpha_{iso}^{l} F\left(\delta_p\right)}{f\left(\xi\right)\left(\left(\lambda - \kappa\right) F\left(\delta_p\right) - \kappa C\right)} \tag{4}$$

where according to (Gallipoli et al., 2003),

$$f(\xi) = 1 - b_1 \, \dot{c}$$

(5)

with b_1 and b_2 as two fitting parameters. Also, we define

$$F(\delta_p) = \left(1 - \left(sgn\,\delta_p\right)|\delta_p|^{\theta}\right), \quad C = -e\frac{\partial f(\xi)}{\partial e}\frac{1}{f(\xi)}F(\delta_p), \quad \text{and} \quad \kappa = \frac{p'}{K}\frac{1+e}{e}$$

where θ is a material parameter, and sgn represents the sign function. Also, by taking α_k as the kinematic hardening parameter and M as the slope of the critical state line in the $p'-q$ space (with q being the deviatoric stress), $\delta_p^{\square}$ is defined by

$$\delta_p^{\square} = 1 - \frac{p'}{\acute{\alpha}_{iso}^{\square}}\left(1 + 2\frac{\alpha_k^2}{M^2}\right)$$

(6)

where $\acute{\alpha}_{iso}^{\square}$ is the image of the current stress state on a Limiting Compression Curve (LCC) (Ghorbani and Airey, 2021) which is defined as follows

$$\ln e = \ln N_I - \lambda \ln p'$$

(7)

where λ denotes the slope of the LCC in $\ln e - \ln p'$ space, and N_I is a material parameter.

Several key features of the model (hardening, softening, dilatancy) are connected to the critical state line which is assumed to be unique in the space defined by void ratio and p'. The mean effective stress and the void ratio at the critical state, (shown by p_c' and e_c, respectively) have the following relationship

$$\ln e_c = \ln N_c - \lambda \ln\left(p_c' + \alpha_{CSL}^{\square}\right) + \ln f(\xi)$$

(8)

where N_c and $\alpha_{CSL}^{\square}$ are material parameters. The state parameter, ψ which is defined as follows $\psi = e - e_c$ (Been and Jefferies, 1985) will connect the hardening law and flow rule to the critical state as described in the following section. The dilatancy, D is written as

$$D = \frac{d\,\varepsilon_v^p}{d\,\varepsilon_q^p} = L\,A_d\left(M^d - \eta_\sigma\right)$$

(9)

where A_d quantifies the magnitude of dilation and is assumed to be a function of soil fabrics as outlined by Dafalias and Taiebat (2016) and Ghorbani and Airey (2021), $L = 1$ or -1 when $\eta_\sigma - \alpha_k \geq 0$ and $\eta_\sigma - \alpha_k < 0$, respectively. M^d is also defined by

$$M^d = M \exp\left(n^d \psi\right)$$

(10)

where $n^d \geq 0$ is a material parameter. The kinematic hardening can evolve when the deviatoric plastic strain, ε_q^p changes as follows

$$\frac{\partial \alpha_k}{\partial \varepsilon_q^p} = h(M^b - \eta_\sigma) \tag{11}$$

where M^b connects the hardening law to the state parameter and the critical state line according to the following equation

$$M^b = M \exp\left(\langle -n^b \psi \rangle\right) \tag{12}$$

where n^b is a material parameter and $\langle \rangle$ denotes the MacCauley brackets. Note that both softening and hardening can be simulated by Equation (11). If $\eta_\sigma > M^b$, softening will occur and if $\eta_\sigma < M^b$, hardening will be predicted. It may also be noted that in the special case of the critical state, $\psi = 0$, hardening will cease as expected by experimental evidence. A smooth convergence of M^b to M is provided when $\psi = 0$ according to Equation (12). In order to have the forgoing hardening and softening mechanism, it must be guaranteed that h will always stay positive. h is defined by

$$h = h_0 G_0 (1 - c_h e) \left(\frac{p'}{p_{atm}}\right)^{\frac{-1}{2}} \frac{1}{\left|a_k - a_k^\iota\right|} \tag{13}$$

where $h_0 \geq 0$ is a material parameter. c_h regulates the contribution of void ratio in the hardening law, and a_k^ι is the kinematic hardening parameter at the initiation of a loading process. a_k^ι will be updated to a_k when a reversal begins.

Moreover, the plastic modulus, K_p has two terms corresponding to the isotropic and kinematic hardening rules and is defined as

$$K_p = \frac{-\partial f}{\partial \alpha_k} \frac{\partial \alpha_k}{\partial \varepsilon_q^p} G_q^\sigma - \frac{\partial f}{\partial \alpha_{iso}^l} \frac{\partial \alpha_{iso}^l}{\partial \varepsilon_v^p} G_v^\sigma \tag{14}$$

where G_q^σ and G_v^σ are the gradient of the plastic potential with respect to q and p', respectively.

The susceptibility of the model to overshooting may be noted in Equations (13) and (14). Upon reversals $a_k^\iota = a_k$ and $K_p \rightarrow \infty$, leading to a pseudo-elastic response at the initiation of loading reversals. If numerical oscillations trigger such an update in a_k^ι, a very stiff behaviour for soils is predicted (since the plastic modulus is a very large value) and therefore, a discontinuity can occur in the stress-strain path. Fig. 1 demonstrates an example of overshooting predicted by the model. This is a simulation of the response of a fully saturated soil with an initial void ratio of 0.735 and the mean effective stress of 100 kPa to triaxial shearing under undrained conditions. The test is simulated by using strain increments of 0.00001. The parameters of the mechanical model were taken from (Ghorbani and Airey, 2021). All the material parameters in this

example and the subsequent simulations in the paper are summarised in Appendix A. It is also notable that an adaptive explicit stress integration scheme is used for this model that was developed by Ghorbani and Airey (2021), and the stress integration tolerance was set to 10^{-5} in all the examples.

The black solid line shows a continuous stress-strain path if no oscillation is induced to the analysis. The green dashed line shows the consequence of inducing a small oscillation in the stress-strain path. To simulate this path, upon reaching the axial strain of 0.1, a small reversal/reading event (the axial strain in both loading stages is set to 0.015%) is induced to represent numerical oscillations. A drastic jump in the predicted deviatoric stress can be seen where the oscillation is induced as a result of the stiff behavior of the soils during the induced oscillation. On the same graph, the performance of a remedy for the stress overshooting effect is demonstrated. This approach follows the proposed method by Dafalias and Taiebat (2016) by defining a "threshold" for the equivalent deviatoric plastic strain during a loading process, $\acute{\varepsilon}_q^p$. According to this method, α_i is updated based on a weighted average method as follows:

$$\alpha_i^{(i+1)} = m\,\alpha_i^{(i-1)} + (1-m)\,\alpha^{(i)} \tag{15}$$

where the superscripts $(i-1)$, (i), and $(i+1)$ stand for the loading steps $(i-1)$, (i), and $(i+1)$, respectively. In addition, the weighting coefficient m is computed according to:

$$m = \left\langle 1 - \left(\frac{\varepsilon_q^{p(i)}}{\acute{\varepsilon}_q^p} \right)^j \right\rangle \tag{16}$$

Also, j is a parameter that is set to a default value of 1 (Dafalias and Taiebat, 2016). It should be noted that $\alpha_i^{(i+1)}$ is determined by the weighted contributions of $\alpha_i^{(i)}$ and $\alpha_i^{(i-1)}$.
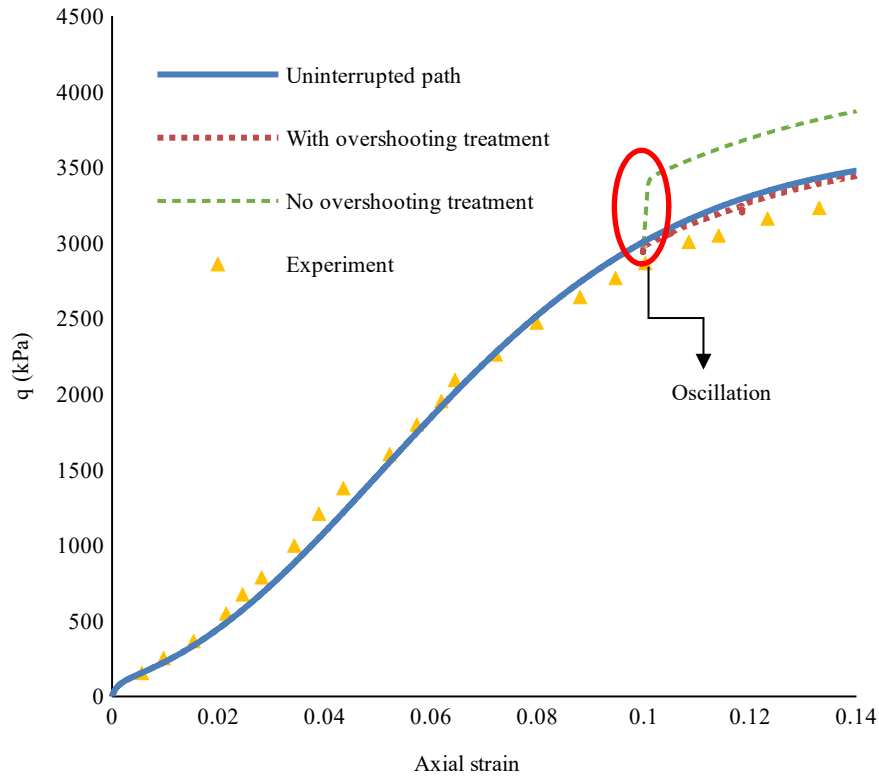
Fig. 1 An example of stress overshooting and the performance of the proposed remedy.

The graph predicted using this remedy is shown in the dotted orange line which denotes a reasonable performance in mitigating the stress overshooting effect since the predicted path almost coincides with the uninterrupted stress-strain path (with no oscillations). It should be noted that the experimental data in this graph is obtained from (Verdugo and Ishihara, 1996).

3 Finite element analysis

A mortar-type discretization (Fischer and Wriggers, 2005, Fischer, 2005, Puso and Laursen, 2004, Bernardi et al., 1993, Ghorbani et al., 2021b) has been used to improve accuracy in the coupled analyses presented here. In the mortar algorithm, a segment-to-segment discretisation is formulated based on the projection of the segments on the surface of one of the interacting bodies onto the segments of the other body. The contact and separation which are governed by the Kuhn–Tucker conditions states

$$t_n \leq 0 \, , g_n \geq 0 \, , t_n \cdot g_n = 0 \qquad\qquad (17)$$

where t_n is the contact stress and g_n represents the normal gap function (Wriggers and Laursen, 2006) used to obtain the minimum distance between two points on the surfaces of the contacting body. By using the penalty method to enforce the constraints, the additional penalty energy from the contribution of the contact segment, i (on boundary Γ_{C_i}¿, Π^{C_i}, to the proposed fully coupled equations can be written as

$$\Pi^{C_i} = \frac{1}{2} \int\limits_{\Gamma_{C_i}}^{\square} \varepsilon_c \, g_n^{\,2} \, d\Gamma \qquad\qquad (18)$$

where ε_c is the penalty coefficient. After linearization and the inclusion of the additional energy arising from the contact in the global governing equation of motion of an unsaturated soil, the finite element discretisation of the above equations can be written as (Ghorbani et al., 2021b)

$$M_u \ddot{U} + C \dot{U} + KU + \dot{c} \, i = 1 \, \dot{c} \, n_s \, K_{N C_i} - Q_w P_w - Q_c^{\dot{c}} P_c \qquad\qquad (19)$$

$$M_w \ddot{U} + Q_w^T \dot{U} + C_{ww} \dot{P}_w + C_{wc} \dot{P}_c + H_{ww} P_w + H_{wc} P_c = \qquad\qquad (20)$$

$$M_c \ddot{U} + R_c^T \dot{U} + C_{cw} \dot{P}_w + C_{cc} \dot{P}_c + H_{wc}^T P_w + H_{cc} P_c = F \qquad\qquad (21)$$

where n_s is the number of contact segments. The symbols F, M, Q, H, and, C in the above equations refer to the force vectors, the mass, coupling, flow, and damping matrices. Furthermore, the symbols $\mathbf{U}, P_w$ and P_c represent displacement, pore water pressure and suction variables. In addition, the superimposed dot denotes the time derivative of a variable. All matrices and force vectors (using the same notations) as well as the definitions of $K_{N C_i}$ and $F_{N C_i}$ are defined in (Ghorbani et al., 2021b) and will not be repeated here for the sake of brevity.

The generalised-α method is used for time integration of the global equations (Ghorbani, 2016, Ghorbani et al., 2016, Ghorbani et al., 2014). In all the following examples the tolerance for the iterative scheme based on the Newton-Raphson method is set to 10^{-3}. Furthermore, the penalty coefficient is set to 10^8 kN/m^3 in the following analyses.

4 Finite element analysis

In this section, we demonstrate the performance of this approach in dynamic contact problems. The problem that is simulated here investigates the response of unsaturated soils to dynamic indentation by a rigid plate under a triangular impact load that involves loading and unloading stages that are shown in Fig. 2. The load has a peak of 6.5 kN and duration of 0.028 s and is applied on a rigid impervious circular plate with a diameter of 300 mm.
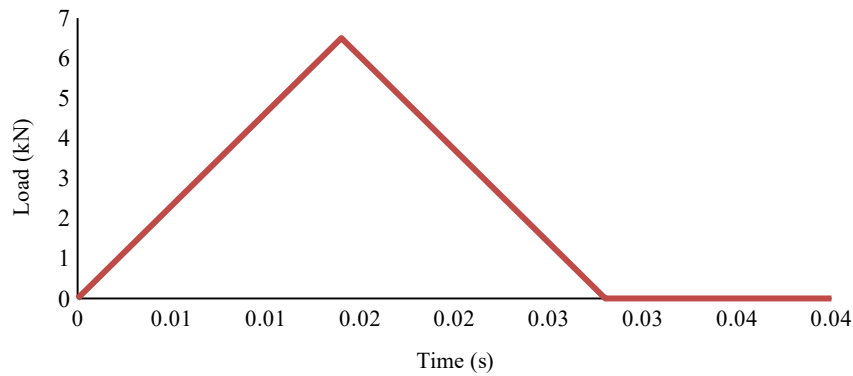

Fig. 2. Load against time.

The problem is idealised as an axisymmetric problem and the soil domain is 2 m by 2 m and is discretised by 900 nodes and 410 fully coupled 6-node axisymmetric elements that take displacement, suction, and pore water pressure fields as unknown variables (Ghorbani et al., 2016, Ghorbani et al., 2020). The side boundary is restrained against horizontal motions and the bottom boundary is restrained against vertical motions. All boundaries are impermeable except the portion of the top boundary that is not in contact with the impervious plate. An initial void ratio of 0.8 is assigned to the soil domain and the at-rest earth pressure coefficient is set to 0.4. The simulations are performed in two steps. In the first step, geostatic stress is established and in the subsequent step, dynamic contact occurs between the plate and the soil. The second step lasts almost 0.04 s and is simulated by using 1333 time steps of the size of 0.00003 s.

Two series of analyses were performed with and without the overshooting treatment, with each series containing eight analyses with different initial suction values (0, 3, 30, 50, 100, 200, 500, and 1000 kPa) being assigned to the entire soil domain while keeping all other analysis and material parameters the constant. We examine the CPU time, the number of iterations in the global generalised-α solver based on Newton-Raphson's method, and the relative difference in the predicted displacement values between the two models.

An example of the measurements at the interface of the contact between the impervious plate and the unsaturated soil with an initial suction of 30 kPa is shown in Fig. 3. The graphs show that upon the impact, pore water pressure increases, suction decreases, and the degree of saturation slightly increases at the interface. The displacement graph also shows a rebound stage initiated at 0.014 s after the impact.

Fig. 4 demonstrates the relative error calculated by Newton-Raphson's method during the first and the second iterations in this analysis. It can be seen that the analysis is relatively stable before the unloading stage begins and the Newton-Raphson method rarely needs a second iteration to satisfy the prescribed convergence criteria. Nonetheless, particularly after the end of the impact, the relative error in the first iterations continues to rise, leading to a need to perform the second iteration to achieve convergence. The increasing need for additional iterations may be noted from the strong oscillations after the impact in the pore water pressure and suction graphs in Fig. 3. Overall, strong oscillations that can be observed during and after the impact makes this problem a good benchmark for evaluating the stability, accuracy, and efficiency of the proposed overshooting remedy.

In terms of the speed of analysis, the selected remedy can have contradictory effects on the stress integration speed and the speed of the generalised-alpha solver that uses Newton Raphson iterations. The method will induce added costs to the integration scheme because of the need to store, recall, and process $\alpha_{\dot{c}}^{(i-1)}$ at every integration point (Note that $\alpha_{\dot{c}}^{(i-1)}$ will become a tensorial quantity in multiaxial space (Ghorbani and Airey, 2021, Dafalias and Taiebat, 2016)). Nonetheless, mitigating the stress overshooting effect can improve the stability of the solution which leads to fewer iterations and overall improvement of the speed of the analysis.
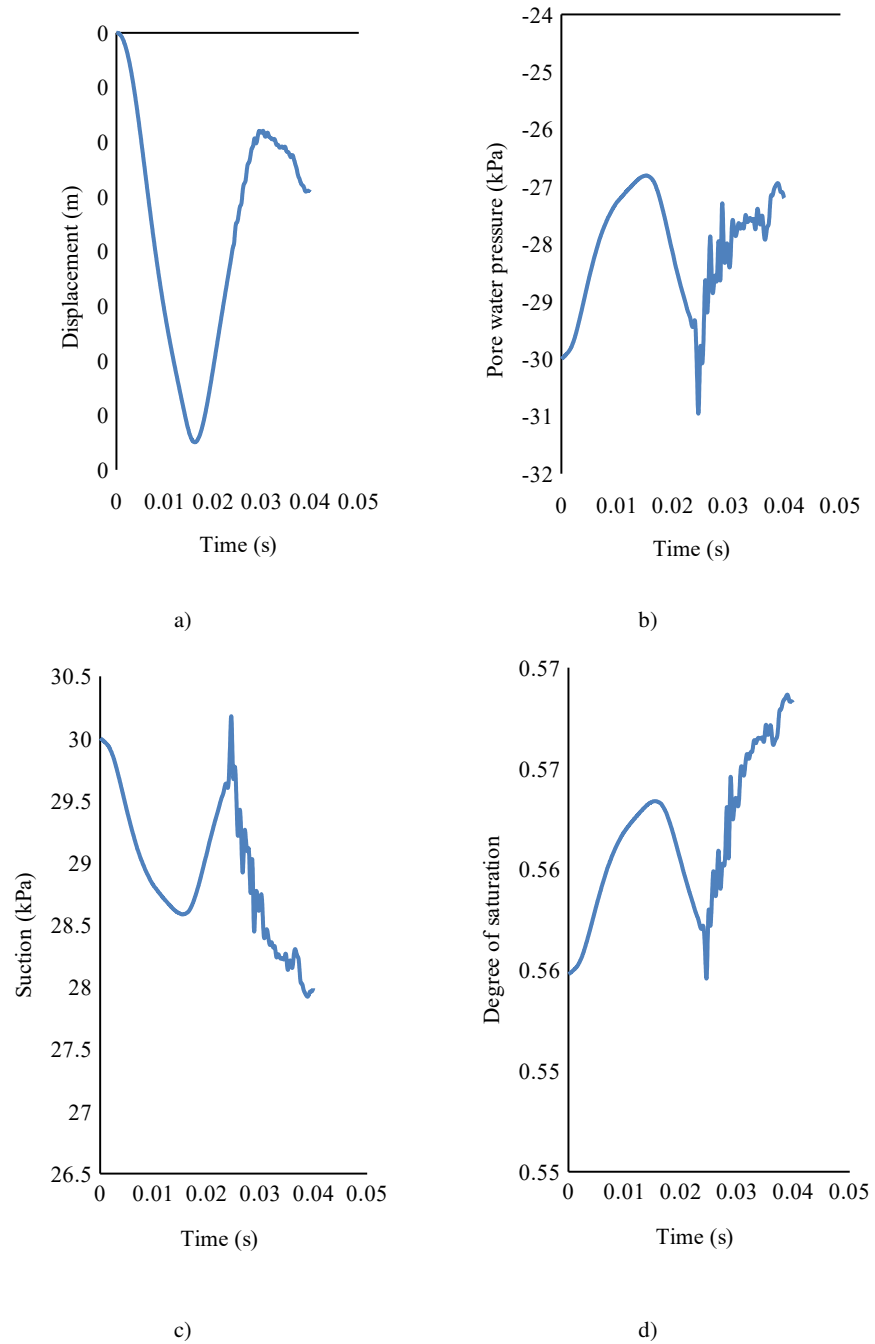
Fig. 3 Model predictions at the contact interface. a) Displacement b) Pore water pressure c) Suction d) Degree of saturation versus time.
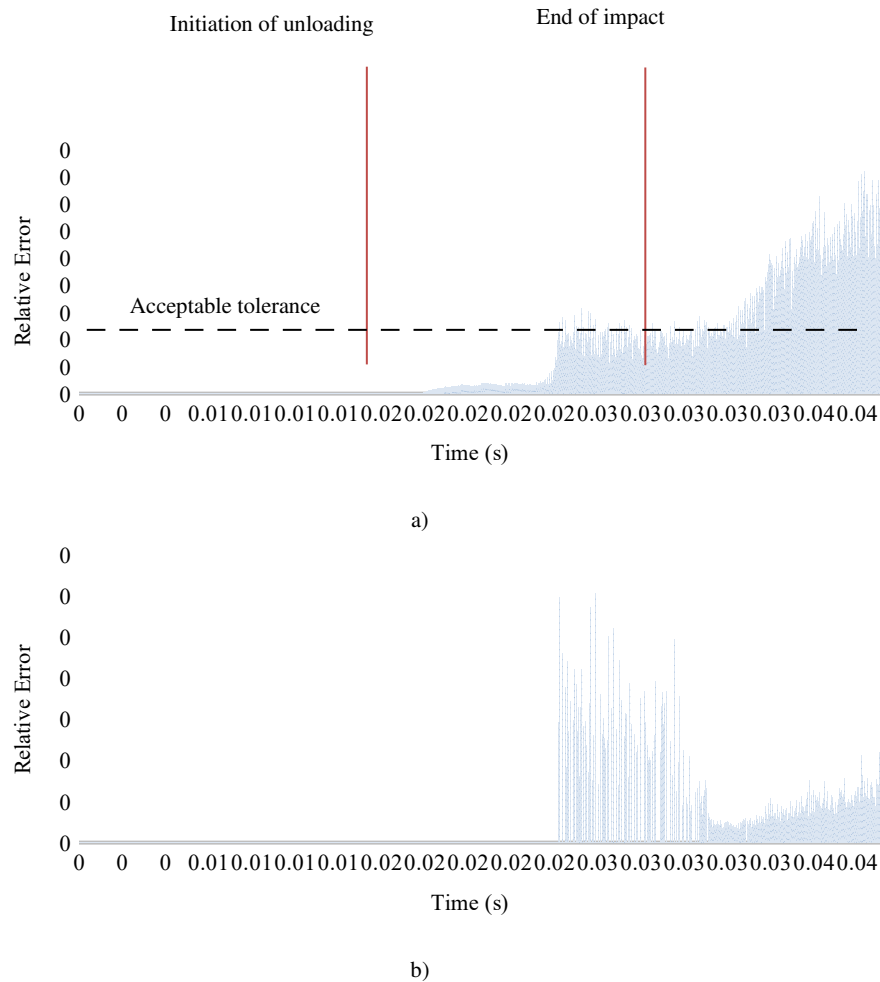
Fig. 4 The relative error in Newton's method in a) First iteration b) Second iteration.

Error: Reference source not found summarises the information on the relative CPU time and the number of iterations in the two series of analyses with and without overshooting treatment. In all studied cases, the use of the proposed overshooting treatment resulted in a decrease in the CPU time although the magnitude of such reduction differs. In the majority of the analyses, fewer iterations were used to achieve the desired convergence when the overshooting treatment was applied. Also, in one instance (initial suction =100 kPa), the use of the selected remedy for overshooting resulted in the successful completion of the analysis, a result that could not be achieved when no overshooting treatment was used.

To investigate the influence of the selected remedy on the predictions, the relative difference between the final displacement in analyses with and without overshooting treatment is considered. The relative displacement is obtained as follows

$$\left| \frac{u_{OS} - u}{u} \right| \tag{22}$$

where u_{OS} and u respectively represent the indentation depths at the end of the analyses with and without the overshooting treatment. It should be noted that when oscillations are not severe (e.g., before the unloading phase as shown in Fig. 4), there is a strong agreement between the two predictions. Nonetheless, the two predictions may diverge toward the end of the analysis as oscillations become more pronounced. An example of the effect of the overshooting treatment on the predicted displacement is shown in Fig. 5. It is seen that before the unloading stage, both graphs are in perfect agreement. Nonetheless, the difference between the two increases as the analysis proceeds.

Table 1 Information on the efficiency of the analyses with and without the overshooting treatment.

Initial suction (kPa)	Relative CPU time	Relative difference of displaceme nt	Iterations (with overshooting treatment)	Iterations (no overshooting treatment)
0	0.68	0.22	1353	1359
3	0.78	0.16	1729	1747
30	0.97	0.00	2071	2085
50	0.96	0.01	1897	2016
100	Unsuccessful analysis when no overshooting treatment is applied.	-	2060	36259 (before termination)
200	0.57	0.81	1333	1801
500	0.78	0.61	1333	1445
1000	0.92	0.09	1333	1333

The relative difference of displacement between the two analyses shows that the selected overshooting treatment can have a drastic effect on the predicted displacement in some cases. The extent of such impact depends on the conditions of the analysis.

5 Conclusions

We have compared the performance of the constitutive model MUD in solving a dynamic contact problem with and without the proposed overshooting treatment. In the studied cases, we have seen an improvement in the speed of the analysis and a reduction of the number of iterations required by the global solver based on the generalized-α scheme and the Newton-Raphson solution method. Nonetheless, the displacements predicted by the two approaches (with and without overshooting treatment) can diverge significantly after the occurrence of loading reversals. The magnitude of the impact has been shown to depend on the initial suction. The extent of the influence of the overshooting treatment on these aspects depends on the initial suction. It should also be noted that other factors such as the size of the time step, the stress integration tolerance, the initial void ratio, the penalty coefficient, as well as the number of elements and integration points may also affect the efficiency of the selected treatment and the conclusions.
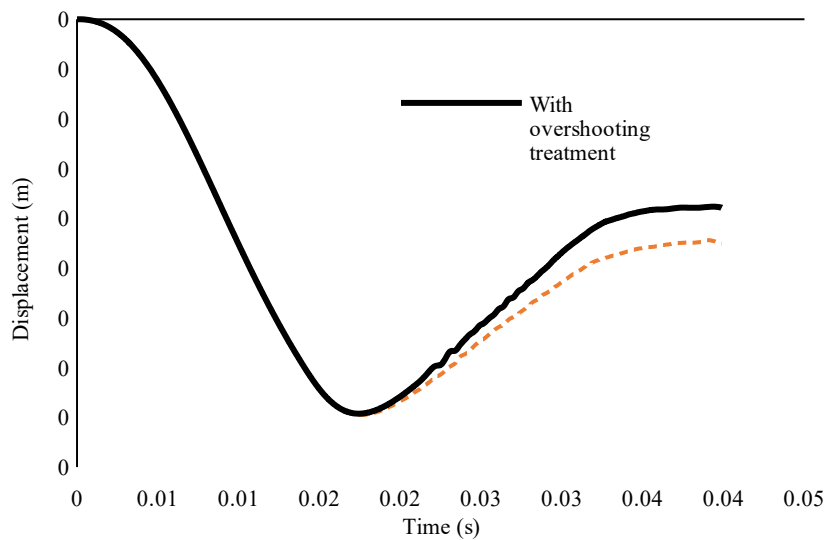

Fig. 5 Displacement at the centre of the impact.

Appendix A   Material parameters

Table 2.General and constitutive material parameters.

Type	Symbol	Value	Unit
Constitutive model parameters	K_0	150	-
	G_0	125	-
	N_l	25	-
	h_0	12.0	-
	c_h	0.968	-
	n^d	2.1	-
	n^b	1.25	-
	A_0	0.4	-
	c_z	600	-
	z_{max}	4	-
	λ	0.37	-
	α_{csl}	3370	kPa
	N_c	18.7	-
	M_c	1.25	-
	c	0.712	-
	b_1	0.5*	-
	b_2	0.5*	-
General material parameters	ρ_s	2700	kg m^{-3}
	ρ_w	997	kg m^{-3}
	ρ_a	1.1	kg m^{-3}
	K_w	2.25×10^6	kPa
	K_a	1.01×10^2	kPa
	k	5×10^{-10}	m^2
	η_w	1.0×10^{-3}	Ns m^{-2}
	η_a	1.8×10^{-5}	Ns m^{-2}

The degree of saturation is assumed to be a function of suction and void ratio following the approach by taking Ω' is a material parameter, we define a modified suction, $p_c^{\dot{c}}$ as follows

$$p_c^{\dot{c}} = p_c \, e^{\Omega'} \tag{23}$$

By ignoring hydraulic hysteresis, by using the modified suction, the equation of the soil-water retention curve (SWRC) is defined by Ghorbani et al. (2018) and Ghorbani and Airey, (2019)

$$S_w^{\square} = S_{rmin} + \left(S_{rmax} - S_{rmin} \right) * \left(\ln \left[\exp(1) + \left(\frac{p_c^{\dot{c}}}{P_a} \right)^{n_x^{\square}} \right] \right)^{-m_x^{\square}} \tag{24}$$

where P_a denotes the air-entry value. $n_x^{\square}$ and $m_x^{\square}$ are the model parameters that control the slope of the SWRC. Also, S_{rmax} and S_{rmin} denote the maximum and minimum values of the residual degree of saturations.

Table 3. SWCC model parameters.

$n_{\square}^{d}$	$m_{\square}^{d}$	P_a(kPa)	Ω'	S_{ι}	S_{rw}
2.0	1.0	5.0	2.0	1	0

References

Airey, D. W., and Ghorbani, J. (2021). Analysis of unsaturated soil columns with application to bulk cargo liquefaction in ships. *Computers and Geotechnics* 140(104402.

Been, K., and Jefferies, M. G. (1985). A state parameter for sands. *Géotechnique* 35(2)**,** 99-112.

Bernardi, C., Maday, Y., and Patera, A. T. 1993. Domain decomposition by the mortar element method. *Asymptotic and numerical methods for partial differential equations with critical parameters.* Springer.

Borja, R. I. (2004). Cam-Clay plasticity. Part V: A mathematical framework for three-phase deformation and strain localization analyses of partially saturated porous media. *Computer Methods in Applied Mechanics and Engineering* 193(48)**,** 5301-5338.

Chen, L., Ghorbani, J., Zhang, C., Dutta, T. T., and Kodikara, J. (2021). A novel unified model for volumetric hardening and water retention in unsaturated soils. *Computers and Geotechnics* 140(104446.

Dafalias, Y. F., and Taiebat, M. (2016). SANISAND-Z: zero elastic range sand plasticity model. *Géotechnique* 66(12)**,** 999-1013.

De Borst, R., Crisfield, M. A., Remmers, J. J., and Verhoosel, C. V. (2012). *Nonlinear finite element analysis of solids and structures*, John Wiley & Sons.

Dong, Y., Lu, N., and Mccartney, J. S. (2018). Scaling shear modulus from small to finite strain for unsaturated soils. *Journal of Geotechnical and Geoenvironmental Engineering* 144(2)**,** 04017110.

Fischer, K., and Wriggers, P. (2005). Frictionless 2D contact formulations for finite deformations based on the mortar method. *Computational Mechanics* 36(3)**,** 226-244.

Fischer, K. A. (2005). *Mortar type methods applied to nonlinear contact mechanics*, Inst. für Baumechanik und Numerische Mechanik, Univ. Hannover.

Gallipoli, D., Gens, A., Sharma, R., and Vaunat, J. (2003). An elasto-plastic model for unsaturated soil incorporating the effects of suction and degree of saturation on mechanical behaviour. *Géotechnique.* 53(1)**,** 123-136.

Ghorbani, J. (2016). *Numerical simulation of dynamic compaction within the framework of unsaturated porous media.* Doctor of Philosophy, University of Newcatsle.

Ghorbani, J., and Airey, D. W. 2019. Some Aspects of Numerical Modelling of Hydraulic Hysteresis of Unsaturated Soils. *In:* HERTZ, M. (ed.) *Unsaturated Soils: Behavior, Mechanics and Conditions.* Nova Science Publishers.

Ghorbani, J., and Airey, D. W. (2021). Modelling stress-induced anisotropy in multi-phase granular soils. *Computational Mechanics (In Press)* 67(497-521.

Ghorbani, J., Airey, D. W., Carter, J. P., and Nazem, M. (2021a). Unsaturated soil dynamics: Finite element solution including stress-induced anisotropy. *Computers and Geotechnics* 133(104062.

Ghorbani, J., Airey, D. W. , and El-Zein, A. (2018). Numerical framework for considering the dependency of SWCCs on volume changes and their hysteretic responses in modelling elasto-plastic response of unsaturated soils. *Computer Methods in Applied Mechanics and Engineering* 336(80-110.

Ghorbani, J., Nazem, M., and Carter, J. (2014). Application of the generalised-α method in dynamic analysis of partially saturated media. *Computer Methods and Recent Advances in Geomechanics***,** 129.

Ghorbani, J., Nazem, M., and Carter, J. (2016). Numerical modelling of multiphase flow in unsaturated deforming porous media. *Computers and Geotechnics* 71(195-206.

Ghorbani, J., Nazem, M., and Carter, J. P. (2020). Dynamic Compaction of Clays: Numerical Study Based on the Mechanics of Unsaturated Soils. *International Journal of Geomechanics* 20(10)**,** 04020195.

Ghorbani, J., Nazem, M., Kodikara, J., and Wriggers, P. (2021b). Finite element solution for static and dynamic interactions of cylindrical rigid objects and unsaturated granular soils. *Computer Methods in Applied Mechanics and Engineering* 384(113974.

Khosravi, A., and Mccartney, J. (Year) Published. Impact of stress state on the dynamic shear moduli of unsaturated, compacted soils. 4th Asia-Pacific conference on unsaturated soils, 2009. 23-25.

Khosravi, A., and Mccartney, J. S. (2012). Impact of hydraulic hysteresis on the small-strain shear modulus of low plasticity soils. *Journal of Geotechnical and Geoenvironmental Engineering* 138(11)**,** 1326-1333.

Kodikara, J., Islam, T., and Sounthararajah, A. (2018). Review of soil compaction: History and recent developments. *Transportation Geotechnics* 17(24-34.

Puso, M. A., and Laursen, T. A. (2004). A mortar segment-to-segment frictional contact method for large deformations. *Computer methods in applied mechanics and engineering* 193(45-47)**,** 4891-4913.

Richart, F. E., Hall, J. R. , and Woods, R. D. (1970). Vibrations of soils and foundations.

Rong, W., and Mccartney, J. (2020). Drained seismic compression of unsaturated sand. *Journal of Geotechnical and Geoenvironmental Engineering* 146(5)**,** 04020029.

Rong, W., and Mccartney, J. (2021). Undrained Seismic Compression of Unsaturated Sand. *Journal of Geotechnical and Geoenvironmental Engineering* 147(1)**,** 04020145.

Rong, W., and Mccartney, J. S. (Year) Published. Effect of Suction on the Drained Seismic Compression of Unsaturated Sand. E3S Web of Conferences, 2019. EDP Sciences, 08004.

18

Schrefler, B. A. (1984). *The Finite Element Method in Soil Consolidation: (with Applications to Surface Subsidence).* PhD, University College of Swansea.

Taiebat, M., and Dafalias, Y. F. (2008). SANISAND: Simple anisotropic sand plasticity model. *International Journal for Numerical and Analytical Methods in Geomechanics* 32(8)**,** 915-948.

Verdugo, R., and Ishihara, K. (1996). The steady state of sandy soils. *Soils and foundations* 36(2)**,** 81-91.

Wriggers, P., and Laursen, T. A. (2006). *Computational contact mechanics*, Springer.